I.A. LYASHENKO,[1,2] N.N. MANKO [1]

[1] Sumy State University
(2, Rimskii-Korsakov Str., Sumy 40007, Ukraine; e-mail: nabla04@ukr.net, mtashan@rambler.ru)
[2] Peter Grünberg Institut-1
(FZ-Jülich, 52425 Jülich, Germany)

PACS 05.70.Ln; 47.15.gm; 62.20.Qp; 68.35.Af; 68.60.-p

ANALYSIS OF THE STABILITY OF STATIONARY BOUNDARY FRICTION MODES IN THE FRAMEWORK OF A SYNERGETIC MODEL

A synergetic model describing the state of an ultrathin lubricant layer squeezed between two atomically smooth solid surfaces operating in the boundary friction mode has been developed further. To explain the presence of different operation modes of the system for various sets of its main parameters, the mathematical analysis of the synergetic model is carried out. The type of functioning a tribological system is described in accordance with the stability character of singular points, and the diagrams distinguishing various operation modes are obtained. Phase portraits corresponding to different stability types are plotted for all diagram areas. A stick-slip mode of motion that is often observed experimentally is described.

K e y w o r d s: boundary friction, friction force, shear stresses, strange attractor, Lorenz system.

1. Introduction

Recently, the processes of boundary friction in nano-sized tribological systems have become a rather interesting object of researches for theorists and experimenters [1–5]. Any system, in which the processes running at the friction of contacting bodies are essential, can be regarded as tribological [1]. The case of atomically smooth solid surfaces, which move relatively to each other with the ultrathin layer of a homogeneous lubricant between them and provided that the distance between the surfaces is fixed, has not been studied in detail. The application of such systems for designing a high-precision equipment and devices [6] increases the interest in this subject. Note that the nano-sized systems reveal abnormal properties in comparison with ordinary macroscopic tribological units. The majority of works devoted to this topic have a fundamental character [7–9]. In comparison with bulk lubricants, the ultrathin lubricant layers are characterized by different melting and solidification temperatures; they have a nonmonotonous dependence of the friction force on the velocity, which follows from the possibility for a lubricant to be in a number of structural states.

One of the bright peculiarities inherent to systems with dry friction is the stick-slip mode of motion [3,10,11]. This mode has a lot of specific features and remains unstudied in detail till now despite a considerable number of theoretical and experimental works (see, e.g., works [12, 13] and the references therein). Since the corresponding experiment in this mode is a complicated task, the stick-slip mode is often studied with the use of a computer-assisted simulation [12, 13]. Work [13] was devoted to the research of the temperature influence on the emergence of the

[1] Below, we consider two elastic contacting solids under loading and in a state of relative motion, with the thin film of a lubricant between them.

boundary friction mode. In work [10], it was shown experimentally and theoretically that the stochastic component of this mode (the time intervals between the beginning moments of the sticking and slipping modes) is controllable, so that the periods of the stick-slip mode can be synchronized by changing the magnitude of a shear force.

Plenty of experimental works formed a basis for the creation of various theoretical models that describe the boundary friction processes [7, 8, 14–17]. One should bear in mind that even minor changes in both the internal (lubricant type [4], structure of friction surfaces, pressure, and so on) and external (loading on the surfaces, the shear velocity, the type of tribological system) parameters can affect the properties of nano-sized systems. For today, the experimental works provide information concerning such main properties of a lubricant as its thickness (the number of molecular layers), temperature, external loading, effective viscosity, elastic and viscous components of shear stresses, and others [6].

In this connection, there appear a considerable number of phenomenological models. One of them was developed in works [18–20], where, in the framework of a synergetic representation of boundary friction and with the use of three differential equations for the stresses, strains, and temperature in the lubricant layer, the nontrivial behavior of a lubricant at the relative motion of rubbing surfaces was described. However, the influence of the parameters in this model on the kinetic modes of dynamic friction has not been studied in detail. In our previous work [21], we showed that the synergetic model allows the stationary stick-slip mode of boundary friction to be described in the deterministic case. This work is a continuation of work [21]. Here, we will study the types of stationary state stability and construct the phase diagrams for various functioning modes of tribological systems.

2. Basic Equations and Stability Analysis

The system of basic equations looks like [18–20]

$$\dot{\sigma} = -\sigma + g\varepsilon, \tag{1}$$

$$\tau\dot{\varepsilon} = -\varepsilon + (T-1)\sigma, \tag{2}$$

$$\delta\dot{T} = (T_e - T) - \sigma\varepsilon + \sigma^2, \tag{3}$$

where σ is the shear component of stresses that arise in the lubricant, ε the shear component of relative deformations, T the lubricant temperature, and T_e the temperature of friction surfaces. The equations also include the constant $g < 1$, which is numerically equal to the ratio between the shear lubricant modulus G and its characteristic value G_0, and the parameters

$$\tau = \tau_\varepsilon/\tau_\sigma, \quad \delta = \tau_T/\tau_\sigma, \tag{4}$$

where τ_σ and τ_ε are the relaxation times for the stresses σ and the strains ε, respectively; and the relaxation time for the temperature, τ_T, is determined by the relation

$$\tau_T = \rho h^2 c_v/\kappa, \tag{5}$$

where ρ is the lubricant density, h the lubricant layer thickness, c_v the specific heat capacity, and κ the thermal conductivity. The stress σ, strain ε, temperature T, and time t in the system of equations (1)–(3) are reckoned in the corresponding units [19]

$$\sigma_s = \left(\frac{\rho c_v \eta_0 T_c}{\tau_T}\right)^{1/2}, \quad \varepsilon_s = \frac{\sigma_s}{G_0}, \quad T_s = T_c, \quad t_s = \tau_\sigma, \tag{6}$$

where T_c is the critical temperature, $G_0 = \eta_0/\tau_\varepsilon$ is a characteristic value of shear modulus, and η_0 is a characteristic value of shear viscosity. The latter is expressed in terms of the actual, dimensional viscosity η as follows [22]:

$$\eta = \frac{\eta_0}{T/T_c - 1}. \tag{7}$$

Hence, $\eta = \eta_0$ at the dimensional temperature $T = 2T_c$ or the dimensionless one $T = 2$.

In works [18–20], it was shown that the zero stationary stresses correspond to a solid-like lubricant structure, whereas, at $\sigma_0 \neq 0$, the lubricant melts and transforms into a liquid-like state. One of the reasons is that, according to the Stribeck–Hersey diagram generalized onto the boundary mode [23], the growth of viscous stresses

$$\sigma_v = F_v/A \tag{8}$$

is accompanied by the growth of the viscous friction force

$$F_v = \eta_{\text{eff}} V A/h, \tag{9}$$

where V is the relative velocity of friction surfaces, η_{eff} the effective viscosity, and A the contact area. From Eqs. (8) and (9), we obtain the following expression for the velocity:

$$V = \sigma_v h/\eta_{\text{eff}}. \tag{10}$$

Since the stress σ in the proposed model is a sum of the viscous and elastic components [19], and the viscous stresses prevail in the liquid-like lubricant layer, the velocity of motion of shear surfaces increases with σ, which corresponds to the kinetic slipping mode and the liquid-like lubricant structure. At $\sigma = 0$, the friction surfaces do not move, which corresponds to their "sticking" owing to the solidification of the layer between the surfaces. Those conclusions are confirmed both theoretically [7] and experimentally [5].

The initial system of equations (1)–(3) has a general character; it does not make allowance for the properties of a specific tribological system. Therefore, it can describe the features of the boundary mode in tribological systems of various types. Let us consider two of them, which are the most widespread (Fig. 1).

Figure 1, *a* schematically illustrates a system consisting of a spring with the stiffness constant k and connected with a block of mass M located on a smooth motionless surface; a lubricant layer of thickness h separates the block and the surface. An additional loading L is applied normally to the block. The free end of the spring moves at the velocity V_0. The system depicted in Fig. 1, *b* is composed of a spring connected to a block on rollers (the rolling friction of the rollers is neglected). Another block is located on the surface of the first block. The velocity of the motion of the second block, V_0, changes periodically [9, 24]. Provided that there is an ultrathin lubricant layer between blocks' surfaces, the motion of the upper block stimulates the lower one to move, with the time dependence of the motion velocity for the lower block, $V(t)$, depending substantially on the friction mode.

Note that the system exhibited in Fig. 1, *a* was studied both experimentally and in the framework of two thermodynamic models [17, 25] basing on the Landau theory of phase transitions, as well as in the framework of a stochastic model, which takes the interaction between the friction surfaces into consideration [8]. In contrast to work [25], the model analyzed in work [17] makes allowance for the influence

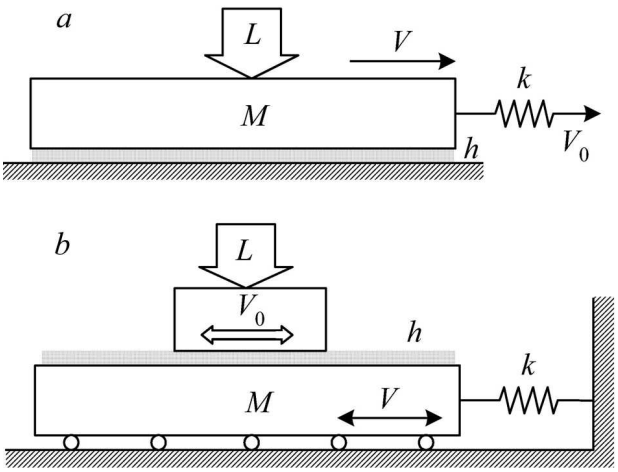

Fig. 1. Mechanical analogs of tribological systems of two types

of the external loading L explicitly. The installation depicted in Fig. 1, *b* was studied experimentally in work [9] and analyzed in the framework of a thermodynamic model in work [24].

The solution of the system of differential equations (1)–(3) in a vicinity of the stationary state is sought in the form

$$\sigma = \sigma_0 + \alpha e^{\lambda t}, \tag{11}$$

$$\varepsilon = \varepsilon_0 + \beta e^{\lambda t}, \tag{12}$$

$$T = T_0 + \gamma e^{\lambda t}, \tag{13}$$

where λ is an unknown increment, the parameters σ_0, ε_0, and T_0 correspond to the stationary state, and the amplitudes α, β, and γ characterize small deviations from this state. Substituting Eqs. (11)–(13) into system (1)–(3), we arrive at a system of algebraic equations

$$\alpha\lambda e^{\lambda t} = -\sigma_0 - \alpha e^{\lambda t} + g\left(\varepsilon_0 + \beta e^{\lambda t}\right), \tag{14}$$

$$\tau\beta\lambda e^{\lambda t} = -\varepsilon_0 - \beta e^{\lambda t} +$$

$$+ \left(T_0 + \gamma e^{\lambda t} - 1\right)\left(\sigma_0 + \alpha e^{\lambda t}\right), \tag{15}$$

$$\gamma\lambda e^{\lambda t} = T_e - T_0 - \gamma e^{\lambda t} - \left(\sigma_0 + \alpha e^{\lambda t}\right)\left(\varepsilon_0 + \beta e^{\lambda t}\right) +$$

$$+ \left(\sigma_0 + \alpha e^{\lambda t}\right)^2. \tag{16}$$

The roots of this system at $(\alpha, \beta, \gamma) \to 0$ are stationary values. The analysis of Eqs. (14)–(16) allows us

to define the critical temperature T_{c0}. Namely, if the temperature of friction surfaces, T_e, is lower than

$$T_{c0} = 1 + g^{-1}, \tag{17}$$

the stationary values

$$\sigma_0 = \varepsilon_0 = 0, \quad T_0 = T_e, \tag{18}$$

are realized, whereas at $T_e > T_{c0}$, either of two sets, $(\sigma_0^+, \varepsilon_0^+, T_0)$ or $(\sigma_0^-, \varepsilon_0^-, T_0)$, where

$$\begin{aligned} \sigma_0^{\pm} &= \pm\sqrt{\frac{gT_e - 1 - g}{1 - g}}, \\ \varepsilon_0^{\pm} &= \pm\frac{1}{g}\sqrt{\frac{gT_e - 1 - g}{1 - g}}, \quad T_0 = 1 + g^{-1}, \end{aligned} \tag{19}$$

is established depending on the initial conditions; the both correspond to the liquid-like friction mode. Hence, at $T_e > T_{c0}$ (see Eq. (17)), the lubricant melts [18–20].

In a first order of smallness with respect to the parameters α, β, and γ, the system of equations (14)–(16) reads

$$(\lambda + 1)\alpha - g\beta = 0, \tag{20}$$

$$(1 - T_0)\alpha + (\tau\lambda + 1)\beta - \sigma_0\gamma = 0, \tag{21}$$

$$(2\sigma_0 - \varepsilon_0)\alpha + \sigma_0\beta + (\delta\alpha + 1)\gamma = 0, \tag{22}$$

where σ_0, ε_0, and T_0 are the stationary values. Therefore, the solutions of the system for T_e above and below the critical value (17) are different. Let us consider firstly the temperature interval $T_e < T_{c0}$ (the solid-like lubricant). In this case, the stationary state (18) is realized. A nontrivial solution of the system of equations (20)–(22) exists if the determinant equals zero,

$$(\delta\lambda + 1)\left[\tau\lambda^2 + (\tau + 1)\lambda + g(1 - T_e) + 1\right] = 0. \tag{23}$$

Equation (23) has the following three roots:

$$\begin{aligned} \lambda_{1,2} &= \frac{-(\tau + 1) \pm \sqrt{\tau^2 + (4gT_e - 4g - 2)\tau + 1}}{2\tau}, \\ \lambda_3 &= -1/\delta, \end{aligned} \tag{24}$$

so that the root λ_3 is always negative. Concerning two other roots, which are complex-conjugate with respect to each other, their real part is also always negative. The form of a root governs the type of stability of a stationary point (see below).

In the liquid-like state of the lubricant ($T_e > T_{c0}$), the stationary values (19) are realized. In this case, substituting those values into system (20)–(22) and equating the corresponding determinant to zero, we obtain the cubic equation

$$\lambda^3 + A\lambda^2 + B\lambda + C = 0 \tag{25}$$

with the coefficients

$$\begin{aligned} A &= 1 + \tau^{-1} + \delta^{-1}, \\ B &= \delta^{-1} + \frac{g(2 - T_e)}{\tau\delta(g - 1)}, \\ C &= \frac{2\,(gT_e - 1 - g)}{\tau\delta}. \end{aligned} \tag{26}$$

We now write the discriminant of Eq. (25):

$$\Delta = -4A^3C + A^2B^2 - 4B^3 + 18ABC - 27C^2. \tag{27}$$

If $\Delta > 0$, Eq. (25) has three different real-valued roots. The equality $\Delta = 0$ means that two real roots coincide. At $\Delta < 0$, we have one real and two complex-conjugate roots.

To analyze eigenvalues (24) and the solution of Eq. (25), let us plot a diagram, where the regions would be characterized by different λ_i-values (Fig. 2). The curve separating regions 1 and 5 in Fig. 2, *a* can be found by analyzing solution (24), because $T_e < T_{c0}$ in this region. In all figures, regions 1 and 2 are separated by condition (17) (dashed curves). The analysis of discriminant (27) (the equation $\Delta = 0$) allows us to plot the curve that separates region 2 from region 3. Let us introduce the additional condition $AB = C$ (see Eq. (26)), which allows us to plot the curve, where the system loses its stability.[2] In Fig. 2, *a*, it is a curve that separates regions 3 and 4. The presence of the complex part and the sign of λ_i determine the type of a singular point for the given set of parameters T_e, g, τ, and δ. In other words, the type of a stationary mode at fixed model parameters can be sometimes determined beforehand, if the λ_i-values are known. In Fig. 2, *a*, there exist five regions for

[2] In this case, Eq. (25) can be written down in the form $(\lambda - a)(\lambda - bI)(\lambda + bI) = \lambda^3 - a\lambda^2 + b^2\lambda - ab^2$, where a and b are real numbers, and I is the imaginary unity. The given condition can be expressed in the form $AB = C$ with the coefficients $A = -a$, $B = b^2$, and $C = -ab^2$.

the selected set of parameters. In regions 1 and 5, the singularity point has coordinates (18), and the corresponding eigenvalues are determined by Eq. (24). Regions 2, 3, and 4 were plotted for the parameter sets, at which $T_e > T_{c0}$; the singularity points (19) are realized in them, and the eigenvalues are determined as the roots of Eq. (25).

In Table, the roots of Eq. (25) are listed, as well as eigenvalues (24) for each of five regions (the corresponding points are marked by diamonds in Fig. 2). In Fig. 2, *a,* three types of singular points are distinguished: stable nodes (regions 1 and 2), stable foci (regions 3 and 5), and a saddle-focus (region 4). Regions with the same stability type correspond to different singular points (the stationary state before (Eq. (18)) and after (Eq. (19)) melting). Region 2 (the stable node) in Fig. 2,*a* is very narrow, but it separates regions 1 and 3 within the whole interval of selected values. For illustration, regions 2 and 5 are shown on a large scale in the inset in Fig. 2, *a* (the T_e-axis contains a break). Figures 2 *b* and *c* are plotted in different coordinates, but include the same regions.

The system of equations (1)–(3) is reduced to a differential equation of the third order [21],

$$\dddot{\sigma} - \ddot{\sigma}\left(\frac{\dot{\sigma}}{\sigma} - 1 - \frac{1}{\tau} - \frac{1}{\delta}\right) - \\ - \frac{\dot{\sigma}}{\tau}\left(\frac{\dot{\sigma}\,(\tau+1)}{\sigma} - \frac{\sigma^2+1+\tau}{\delta}\right) - \\ - \frac{\sigma\left(g\left(T_e+\sigma^2-1\right)-\sigma^2-1\right)}{\tau\delta} = 0. \qquad (28)$$

In this equation, the stresses σ, in accordance with Eq. (10), are proportional to the velocity of relative motion of the friction surfaces, V; therefore, $\dot{\sigma}$ is the acceleration. Let us plot the phase portraits of the system for all regions in the diagram. For this purpose, we should numerically solve Eq. (28) with the use of the Runge–Kutta method of the fourth order and plot figures for the diagram regions with the parameters taken from Table (for all five points). The stable node is shown in Fig. 3. Figure 3, *a* corresponds to the temperature $T_e < T_{c0}$, at which one stationary point (18) is realized (region 1). This case corresponds to the lubricant solidification in time. Figure 3, *b* corresponds to the temperature $T_e > T_{c0}$.

Roots of Eqs. (23) and (25) for various diagram regions shown in Fig. 2

No.	τ	δ	g	T_e	$\lambda_{1,2,3}$	Point type
$1'$	3	0.6	0.2	4	$-1.6667, -1.2244, -0.1089$	stable node
$2'$	20	3	0.5	4	$-1.0489, -0.2771, -0.0573$	stable node
$3'$	3	30	0.2	30	$-1.3431, -0.0118 \pm 0.2816I$	stable focus
$4'$	3	30	0.2	120	$-1.3725, 0.0029 \pm 0.6076I$	saddle-focus
$5'$	3	30	0.8	0.5	$-0.0333, -0.6667 \pm 0.1491I$	stable focus

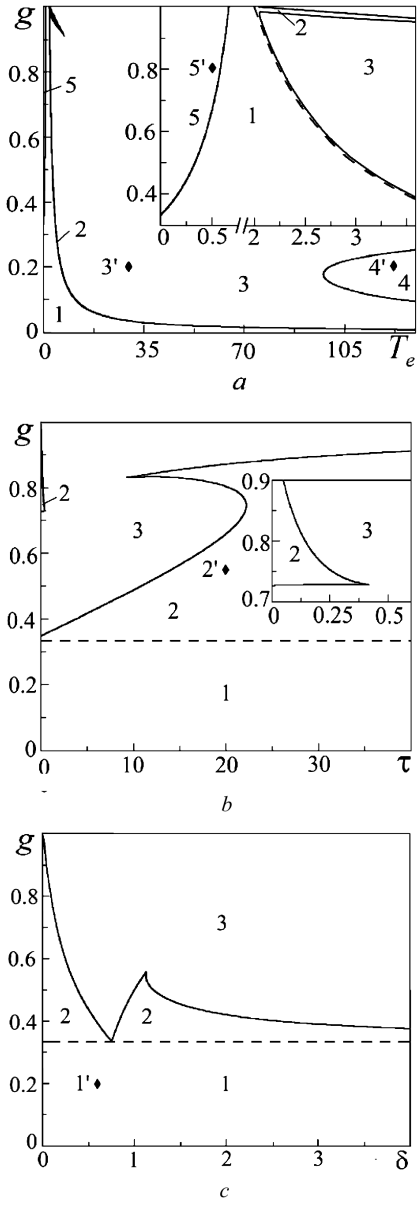

Fig. 2. Diagrams of stability types for singular points: (*a*) $\tau = 3$, $\delta = 30$; (*b*) $T_e = 4$, $\delta = 3$; (*c*) $\tau = 3$, $T_e = 4$

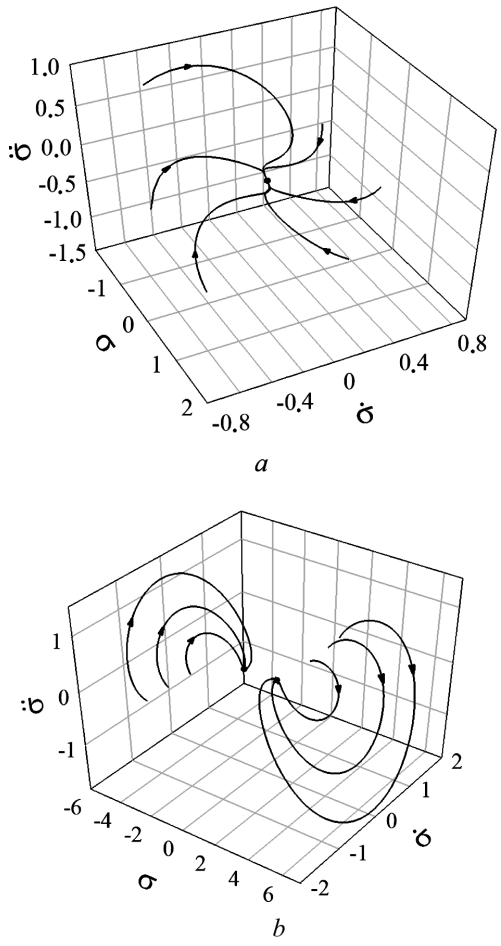

Fig. 3. Phase portraits of Eq. (28) corresponding to the parameters of points $1'$ (a) and $2'$ (b)

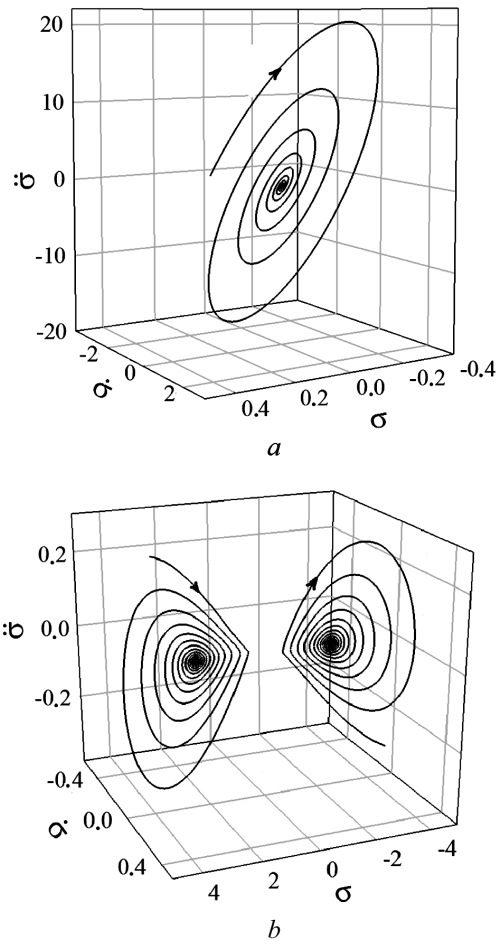

Fig. 4. Phase portraits of Eq. (28) corresponding to the parameters of points $5'$ (a) and $3'$ (b)

At this temperature, two symmetric singular points 19 are realized (region 2), which correspond to the liquid-like lubricant. From the shape of trajectories in Fig. 3, *a*, it follows that, before the stationary state is established (i.e. the system stops), an aperiodic transient mode takes place, in which the stresses relax to the stable value $\sigma = 0$, which corresponds to the solid-like lubricant structure. In this case, the mobile block shown in Fig. 1 stops in due course. It can be realized in the case shown in Fig. 1, *a* at the velocity $V_0 = 0$. This situation also describes the behavior of the system shown in Fig. 1, *b* at $V_0 = 0$, when the lower block is initially not in the equilibrium state, i.e. the spring is either compressed or tensed. In Fig. 3, *b*, the both singular points are equivalent and, as well as in Fig. 3, *a*, correspond to stable nodes. However, for all selected initial conditions, a motion at a constant velocity is eventually established. This situation corresponds to the tribological system exhibited in Fig. 1, *a* at $V_0 \neq 0$. If $\sigma < 0$, the friction surface moves with a negative velocity, i.e. in the opposite direction (the reverse motion).

A convergence in the form of stable focus is also represented by two regions, 3 and 5, where the singular points (19) and (18), respectively, are realized. At the parameters of region 5 (Fig. 4, *a*), the temperature is lower than the melting one; therefore, the trajectories in the phase portrait converge to the singular point (18). The phase portrait depicted in Fig. 4, *b* has the parameters of region 3; therefore, it corresponds to the melted lubricant (two nonzero singular points are realized). For this type of stability, long-

term oscillations take place in the system concerned before a motion with a constant velocity is established (Fig. 4, *b*) or the system stops (Fig. 4, *a*). Moreover, at some parameters, the trajectories do not converge to singular points, but a chaotic mode is realized [21]. In the latter case, to elucidate the features of this mode, an additional analysis is required. In the case shown in Fig. 4, *a*, the mobile block (see Fig.1,*a*) also eventually stops, as in Fig.3, *a*. This situation also describes the behavior of the system shown in Fig. 1, *b* at $V_0 = 0$, when the lower block is initially not in the equilibrium state, i.e. the spring is either compressed or tensed. In due course, when a motion with a constant velocity is established (Fig. 4, *b*), the situation corresponds to the tribological system shown in Fig. 1, *a* at $V_0 \neq 0$.

A convergence of the saddle-focus type can reveal itself as a saddle or a focus, depending on the parameter set selected from the region. The phase portrait exhibited in Fig. 5, *a* is characterized by two symmetric singular points representing unstable foci. The considered diagram region corresponds to condition (19). In this region, the motion with a constant velocity cannot be established because the system enters the chaotic mode of functioning. Hence, the stationary mode is accompanied by permanent phase transitions between the solid-like and liquid-like lubricant states. This mode is not periodic in time but is a strange attractor, i.e. it realizes a deterministic chaotic mode in the system [21]. Since the velocity of the friction block motion permanently changes its sign, the considered situation describes the behavior of the system shown in Fig. 1, *b*, when the motion direction changes under the action of an external influence. However, at large V_0-values, the examined reverse mode can also be realized in the systems, whose analog is shown in Fig. 1, *a*. This occurs because, when the free end of the spring moves at a large velocity V_0, the spring itself has enough time to be strongly stretched within the time interval of the surface "sticking" (i.e. when $\sigma = 0$ and the lubricant is solid-like). On the other hand, as the lubricant melts, the block slides at a large distance owing to a large magnitude of elastic force $k\Delta x$ (Δx is the string elongation), the spring becomes compressed at that, and the direction of the elastic force changes. As a result, the block may move in the opposite direction for some time [21]. Figure 5, *b* (the stationary mode at the parameters of Fig. 5, *a*) exhibits a Lorenz butterfly, which in well-known in the chaos theory [26, 27]. Hence, Fig. 2 reveals the existence of essentially different friction modes. At the same time, this figure also demonstrates that such modes can emerge in tribological systems of various types.

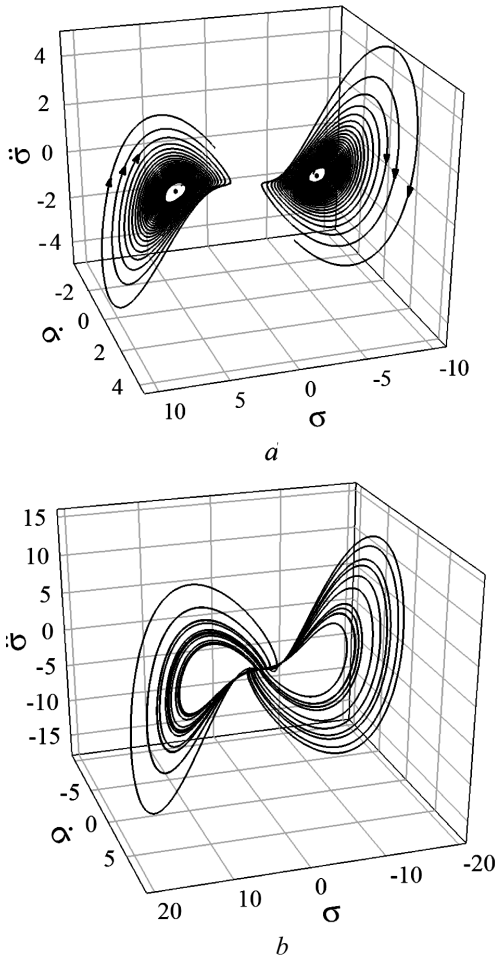

Fig. 5. Phase portraits of Eq. (28) corresponding to the parameters of point $4'$: (*a*) near the singular points and (*b*) in the stationary mode

3. Conclusions

In this work, we made a further research of the synergetic model that describes the state of an ultrathin lubricant layer squeezed between atomically smooth solid surfaces in the course of boundary friction. It is shown that this model can describe the behavior of tribological systems of various types. A number of stationary solutions, which correspond to the dry

and liquid friction modes, are found, as well as the ranges of model parameters, at which that or another mode of tribological system functioning is established. In addition, different modes characterized by one of three types of convergence (a stable node, a stable focus, or a saddle-focus) are distinguished. For each mode, the phase portrait is plotted, and the behavior of tribological system is described. The growth of the friction surface temperature is found to result in an enhancement of the stochasticity in the system. If the temperature exceeds the critical value, the mode of functioning of the system is described by the Lorenz attractor. In a wide range of parameters, the reverse motion of the friction surfaces is realized. The results obtained qualitatively coincide with known experimental data.

The work was sponsored by the State Fund for Fundamental Researches of Ukraine in the framework of the grant of the President of Ukraine GP/F44/010 "Phenomenological theory of boundary friction in tribological nanosystems", No. 0112U007318. Some results were obtained under the support of the Ministry of Education and Science, Youth and Sport of Ukraine in the framework of the project "Simulation of friction of metallic nanoparticles and boundary films of liquids interacting with atomically smooth surfaces", No. 0112U001380. The work was supported by the KMU grant. The research was carried out during the stay of I.A.L. at the Forschungszentrum Jülich (Germany) on the invitation of B.N.J. Persson.

1. B.N.J. Persson, *Sliding Friction. Physical Principles and Applications* (Springer, Berlin, 2000).
2. O.A. Mazyar, G.K. Jennings, and C. McCabe, Langmuir **25**, 5103 (2009).
3. A. Pertsin and M. Grunze, Langmuir **24**, 135 (2008).
4. S. Lee, R. Iten, M. Müller, and N.D. Spencer, Macromolecules **37**, 8349 (2005).
5. Sh. Yamada, Langmuir **21**, 8724 (2005).
6. J. Israelachvili, Surf. Sci. Rep. **14**, 109 (1992).
7. V.L. Popov, Tech. Phys. **46**, 605 (2001).
8. A.E. Filippov, J. Klafter, and M. Urbakh, Phys. Rev. Lett. **92**, 135503 (2004).
9. C.-R. Yang, Y.-C. Chiou, and R.-T. Lee, Tribol. Int. **32**, 443 (1999).
10. R. Capozza, S.M. Rubinstein, I. Barel, M. Urbakh, and J. Fineberg, Phys. Rev. Lett. **107**, 024301 (2011).
11. I.A. Lyashenko, Tech. Phys. **56**, 701 (2011).
12. O.M. Braun and M. Peyrard, Phys. Rev. Lett. **10**, 125501 (2008).
13. A. Benassi, A. Vanossi, G.E. Santoro, and E. Tosatti, Phys. Rev. Lett. **106**, 256102 (2011).
14. S. Ciraci and A. Buldum, Wear **254**, 911 (2003).
15. O.M. Braun and N. Manini, Phys. Rev. E **83**, 021601 (2011).
16. A.I. Volokitin and B.N.J. Persson, Phys. Rev. Lett. **106**, 094502 (2011).
17. I.A. Lyashenko, A.V. Khomenko and L.S. Metlov, Tribol. Int. **44**, 476 (2011).
18. A.V. Khomenko and I.A. Lyashenko, J. Phys. Studies **11**, 268 (2007).
19. A.V. Khomenko, I.A. Lyashenko, and V.N. Borisyuk, Ukr. J. Phys. **54**, 1139 (2009).
20. A.V. Khomenko and I.A. Lyashenko, J. Frict. Wear **31**, 308 (2010).
21. I.A. Lyashenko and N.N. Manko, J. Frict. Wear **34**, 38 (2013).
22. A.I. Olemskoi and E.A. Toropov, Fiz. Met. Metalloved. **9**, 5 (1991).
23. G. Luengo, J. Israelachvili, and S. Granick, Wear **200**, 328 (1996).
24. I.A. Lyashenko, Tech. Phys. **56**, 869 (2011).
25. I.A. Lyashenko, Tech. Phys. **57**, 17 (2012).
26. A.Yu. Loskutov and A.S. Mikhailov, *Principles of the Theory of Complex Systems* (Reg. Stokh. Dinam., Moscow-Izhevsk, 2007) (in Russian)
27. E. Lorenz, J. Atmos. Sci. **20**, 130 (1963).
28. D. Ruelle and F. Takens, Comm. Math. Phys. **20**, 167 (1971).
29. I.A. Lyashenko, A.V. Khomenko, and L.S. Metlov, Tech. Phys. **55**, 1193 (2010).

Received 05.02.13.
Translated from Ukrainian by O.I. Voitenko

Я.О. Ляшенко, Н.М. Манько

АНАЛІЗ СТІЙКОСТІ СТАЦІОНАРНИХ РЕЖИМІВ МЕЖОВОГО ТЕРТЯ В РАМКАХ СИНЕРГЕТИЧНОЇ МОДЕЛІ

Р е з ю м е

У даній роботі проведено подальший розвиток синергетичної моделі, яка описує стан ультратонкого шару мастила, що затиснутий між двома атомарно-гладкими твердими поверхнями, які працюють у режимі межового тертя. Проведено математичний аналіз синергетичної моделі з метою пояснення виникнення різних режимів роботи системи при зміні головних параметрів. Тип функціонування трибологічної системи описаний у відповідності з характером стійкості особливих точок. Отримано діаграми, на яких виділено різні режими роботи. Для всіх областей діаграм побудовано фазові портрети, що відповідають різним типам стійкості. Описано переривчастий рух, що часто зустрічається в експериментах.